ReaxFF Reactive Force Field for the Y-Doped BaZrO₃ Proton Conductor with Applications to Diffusion Rates for Multigranular Systems

Adri C. T. van Duin, Boris V. Merinov, Sang Soo Han, Claudio O. Dorso, and William A. Goddard III*

Materials and Process Simulation Center (139-74), California Institute of Technology, Pasadena, California 91125

Received: February 5, 2008; Revised Manuscript Received: May 14, 2008

Proton-conducting perovskites such as Y-doped BaZrO₃ (BYZ) are promising candidates as electrolytes for a proton ceramic fuel cell (PCFC) that might permit much lower temperatures (from 400 to 600 °C). However, these materials lead to relatively poor total conductivity (~10^{-4} S/cm) because of extremely high grain boundary resistance. In order to provide the basis for improving these materials, we developed the ReaxFF reactive force field to enable molecular dynamics (MD) simulations of proton diffusion in the bulk phase and across grain boundaries of BYZ. This allows us to elucidate the atomistic structural details underlying the origin of this poor grain boundary conductivity and how it is related to the orientation of the grains. The parameters in ReaxFF were based entirely on the results of quantum mechanics (QM) calculations for systems related to BYZ. We apply here the ReaxFF to describe the proton diffusion in crystalline BYZ and across grain boundaries in BYZ. The results are in excellent agreement with experiment, validating the use of ReaxFF for studying the transport properties of these membranes. Having atomistic structures for the grain boundaries from simulations that explain the overall effect of the grain boundaries on diffusion opens the door to in silico optimization of these materials. That is, we can now use theory and simulation to examine the effect of alloying on both the interfacial structures and on the overall diffusion. As an example, these calculations suggest that the reduced diffusion of protons across the grain boundary results from the increased average distances between oxygen atoms in the interface, which necessarily leads to larger barriers for proton hopping. Assuming that this is the critical issue in grain boundary diffusion, the performance of BYZ for multigranular systems might be improved using additives that would tend to precipitate to the grain boundary and which would tend to pull the oxygens atoms together. Possibilities might be to use a small amount of larger trivalent ions, such as La or Lu or of tetravalent ions such as Hf or Th. Since ReaxFF can also be used to describe the chemical processes on the anode and cathode and the migration of ions across the electrode-membrane interface, ReaxFF opens the door to the possibility of atomistic first principles predictions on models of a complete fuel cell.

1. Introduction

Fuel cells provide a most promising alternative to traditional power generation systems. In particular, solid oxide fuel cells (SOFCs) possess a number of advantages including (1) high efficiency, especially when integrated with thermal energy conversion devices utilizing the heat available from SOFCs; (2) fuel flexibility, allowing essentially all hydrocarbon fuels; and (3) compatibility with inexpensive nonprecious metal catalysts.

The main obstacle to the wide commercial utilization of SOFCs is their high cost. This results in part from the high operating temperatures (800−1000 °C) required to obtain sufficiently high oxygen anion diffusion, which places severe restrictions on materials. Therefore, it would be desirable to find an alternative to the standard SOFC electrolyte, yttria-stabilized zirconia (YSZ) that would enable use of reduced temperature operation (500−700 °C).

Promising candidates for lower temperature fuel cell membranes include the family of proton-conducting perovskites. Perovskite oxide materials provide a wide variety of technologically important physicochemical properties, including high-temperature superconductivity, ferroelectricity, piezoelectricity,

and electrical capacity. For many perovskite oxides, acceptor doping (such as Y in place of Zr) leads to high protonic conductivity at elevated temperatures after exposure to water vapor.[1−6] Such materials could enable a dramatic reduction in the operating temperature for fuel cells from that required in commercial SOFCs based on YSZ. In addition, doped perovskite oxides often exhibit very good chemical and mechanical stability, making them attractive for applications in such electrochemical devices as fuel cells, hydrogen sensors for molten metals, H₂/D₂ separators, and hydrogen pumps.

In particular, Y-doped BaZrO₃ (BYZ) is a most promising proton-conducting material for a proton ceramic fuel cell (PCFC), permitting operation at medium temperatures (400−600 °C) while providing such desirable properties as high protonic conductivity and excellent chemical and mechanical stability. Unfortunately, existing BYZ materials have extremely high grain boundary resistance that leads to a relatively poor total conductivity (~10^{-4} S/cm), too low for application of BYZ in a PCFC (which requires >10^{-2} S/cm).

Some progress is being made in improving these materials by changing the conditions and processes for synthesizing them.[7,8] However, the performance remains far from satisfactory. Part of the problem in improving these systems is that it is not known which aspects of the grain boundaries are responsible

ReaxFF Reactive Force Field

J. Phys. Chem. A, Vol. 112, No. 45, 2008 **11415**
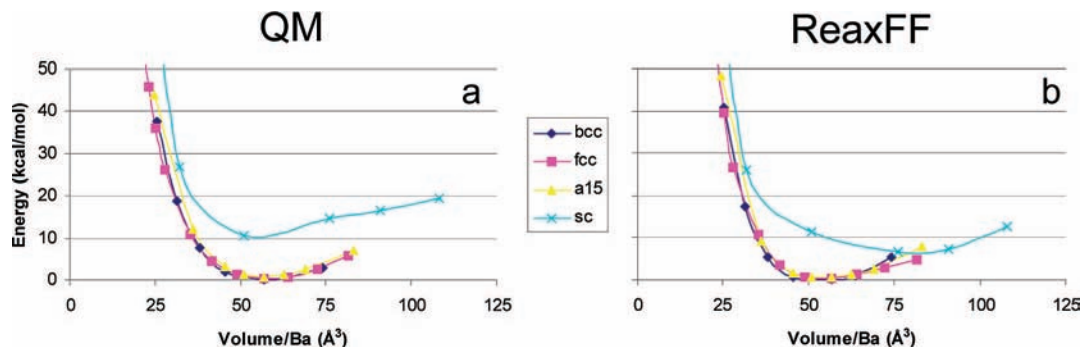
Figure 1. Equations of state for cubic polymorphs of Ba metal from QM and ReaxFF. The ground-state from experiment is bcc. Both QM and ReaxFF predicted that fcc, bcc, and A15 are nearly degenerate.
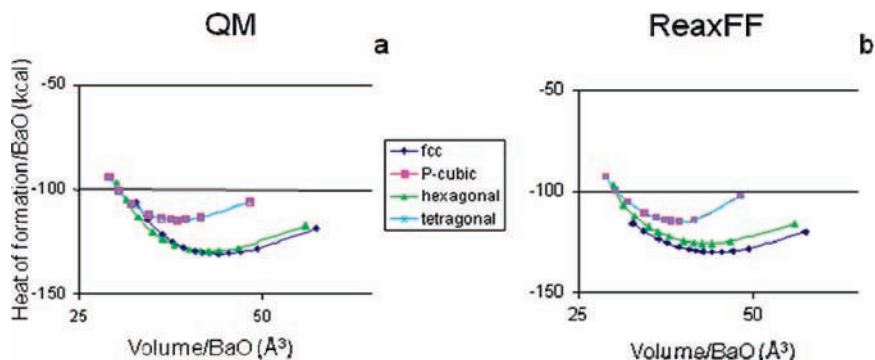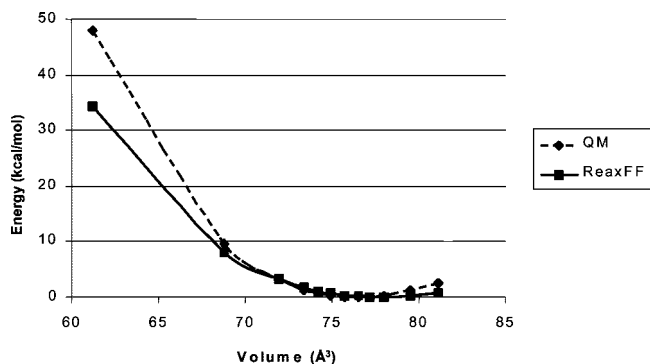

Figure 2. QM- and ReaxFF equations of state for various barium monoxide polymorphs. The ground state from experiment is fcc (the B1 or NaCl structure in which each Ba has six O neighbors), P-cubic denotes the B2 or CsCl structure (each Ba has eight neighbors), hexagonal denotes the nickeline or B3 structure (each Ba has six neighbors), and tetragonal denotes the crystal structure of a high-density BaO-phase[46] or B4-structure (each Ba has eight neighbors). We see that both QM and ReaxFF predict a B1 ground state, with B3 close in energy but B2 and B4 substantially higher. The energies are referenced to PBE calculations on Ba metal and the O_2 molecule. The experimental heat of formation of BaO is -134 kcal/mol at 300 K.

for the very low conductivity. We believe that armed with a mechanism, it might be possible to better suggest changes in the materials and processing to optimize the properties. Unfortunately, the available means of experimentally characterizing these systems provides little guidance for improving them. These questions include

(1) What is the distribution of Ba, Zr, and oxygen in the grain boundary and interface, and how are they affected by doping?

(2) Where does the Y go preferentially, and which O atoms prefer to have the proton?

(3) How do the electrostatic potentials vary across the interface, and how do they depend on doping?

(4) What is the effect of hydrogenation with additional water at the interface and in the grains?

Experiments can sometimes provide some overall estimates of some of these quantities, but it is most difficult to determine from experiment the atomistic structural details at the grain boundaries needed to postulate and test mechanistic ideas.

An alternative to make progress here is to use first-principles-based molecular dynamics and Monte Carlo simulations. Such first principles simulations of reactions and diffusion usually means quantum mechanics (QM, solving the Schrödinger equation), which restricts practical calculations to ∼100 atoms per periodic cell and times of ∼20 ps. Such simulation sizes and times are many orders of magnitude too small to examine the issues relevant to improving grain boundary diffusion in BYZ. Instead, we use such QM calculations to determine the parameters for the ReaxFF reactive force field and then use ReaxFF in long-term MD on large-scale complex systems relevant for BYZ.

Figure 3. Equations of state for the perovskite cubic $BaZrO_3$-phase from QM and ReaxFF.

ReaxFF is based fully on accurate QM and retains nearly the accuracy of QM while allowing large scale MD for computational costs nearly as low as for simple force fields. ReaxFF has been applied to reactive processes for many systems including organic reactions,[9] reactions of energetic materials under extreme conductions,[10,11] decomposition of improvised explosive devices,[12] thermal decomposition of polymers,[13] selective oxidation of propene by $BiMoO_x$ heterogeneous catalysts,[14] catalysis at fuel cell electrodes and proton conductivity of PEM,[15] crack propagation in silicon crystals,[16] dissociation H_2 on Pt surfaces,[17] hydrogen storage in Mg nanoclusters,[18] catalytic formation of carbon nanotubes,[19] and tribology of metal−metal oxide interfaces.[20] Recently, we used ReaxFF to investigate the initial steps of oxidation of O_2 with aromatic and aliphatic systems,[21] showing that ReaxFF may be applied to complex oxidations.

11416 *J. Phys. Chem. A, Vol. 112, No. 45, 2008*

van Duin et al.

We report here the details in developing the parameters in ReaxFF to describe the structures and processes in BYZ. The parameters of ReaxFF were fitted a large variety of QM data on systems related to BYZ, including reactive processes.

In addition, we report the results from using ReaxFF to describe the proton diffusion in crystalline BYZ and across grain boundaries in BYZ. These results are in excellent agreement with experiment, validating the use of ReaxFF for studying the transport properties of these membranes.

Since ReaxFF can also be used to describe the chemical processes on the anode and cathode and the migration of ions across the electrode-membrane interface, ReaxFF opens the door to the possibility of first principles atomistic predictions on models of a complete fuel cell. The studies here include only modestly sized systems and modest periods; however, ReaxFF calculations of reactive processes have already been reported on systems with 1 000 000 atoms.[22] Thus, with currently available computational facilities, one can consider models of a complete fuel cell that include realistic models of the various interfaces and processes. This enables the study of proton transport under realistic conditions.

2. Computational Methods

All QM calculations were performed at $T = 0$ K using density functional theory (DFT). The periodic calculations use the PBE functional[23] based on the generalized gradient approximation (GGA).[24,25] The finite cluster calculations use the hybrid B3LYP functional. B3LYP combines exact Hartree−Fock exchange with the local exchange functional of Slater[26] and includes the Becke nonlocal gradient correction,[27] the Vosko−Wilk−Nusair exchange functional,[28] and the Lee−Yang−Parr local and nonlocal correlation functional.[29] The accuracy of these and other DFT methods is summarized in references 30 and 31.

The Jaguar 5.0 program package[32] was employed for the ab initio cluster calculations. The metals were described using the Hay and Wadt core−valence relativistic effective core potentials (ECP) or pseudopotentials (PP).[33] This potential uses angular momentum projection operators (nonlocal ECP) to enforce the Pauli principle.[34,35] In the Jaguar program package the ECP utilizes the LACVP** basis set. The oxygen atoms were described at the all electron level using a modified variant of the Pople 6−31G** basis set,[36] in which the six d-functions were reduced to five.

The periodic QM calculations were carried out using the SeqQuest code,[37] which uses Gaussian basis functions rather than the plane wave basis often used in periodic systems. Nonlocal ECP or PP[34,35] similar to those in reference 33, but for use in periodic systems, were employed to replace the core electrons. These calculations used "double-ζ plus polarization" contracted Gaussian functions[38] optimized for periodic calculations.

These QM results obtained for relevant condensed phases and cluster systems were then used as described below to derive parameters for the ReaxFF, including the bond order/bond distance relationships. ReaxFF updates bond orders and charges at every MD step, providing a mechanism for bonds to form and break during a simulation.

The ReaxFF was subsequently implemented in MD simulations. In addition, the QM calculations were directly used to gain insight into mechanisms of chemical reactions, local dynamics of proton migration, and surface stabilities. The data from these QM studies are included in the Supporting Information.
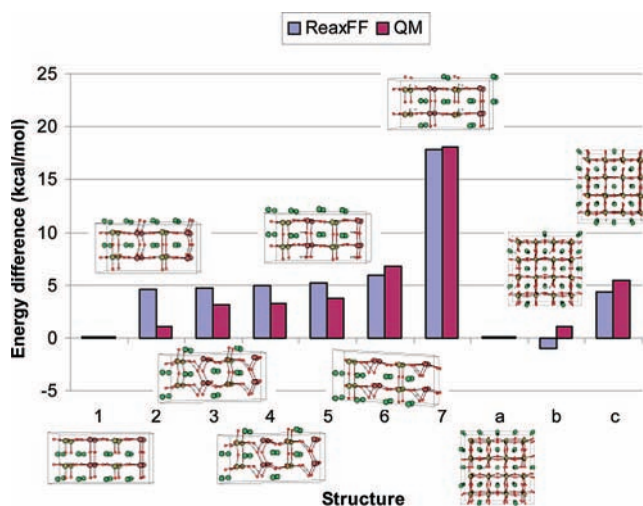
Figure 4. QM- and ReaxFF energies for seven configurations of a 50% YH-exchanged BaZrO$_3$ phase (Ba$_2$ZrYHO$_6$) (1−7) and three configurations of a 12.5% YH-exchanged BaZrO$_3$ phase (Ba$_8$Zr$_7$YHO$_{24}$) (a−c). Configuration 1 has the hydrogen bound to an Y−O−Y oxygen, pointing in the Y-plane. In configuration 2, the hydrogen is shared between 2 Y−O−Y oxygens. Configuration 3 has the hydrogen bound to a Zr−O−Y oxygen and has a short (1.5 Å) contact with a Y−O−Y oxygen. Configuration 4 is a slightly distorted version of configuration 4. Configuration 5 has the hydrogen bound to a Y−O−Y oxygen pointing out of the Y-plane. In configuration 6, the hydrogen is bound to a Zr−O−Y oxygen and has a short contact with a Zr−O−Zr oxygen. Configuration 7 has the hydrogen bound to a Zr−O−Zr oxygen and pointing in the Zr-plane. Configuration (a) has the hydrogen bound to a Zr−O−Zr oxygen in the Zr/Y plane; the hydrogen has a short contact with a Zr−O−Y oxygen. Configuration (b) has the hydrogen bound to a Y−O−Zr oxygen with a short contact to a Zr−O−Zr oxygen. In configuration (c), the hydrogen is bound to a Zr−O−Zr oxygen in the Zr-plane and has a short contact with a Zr−O−Y oxygen. The coordinates for these structures are provided in the Supporting Information.

3. ReaxFF Development

To develop a reliable ReaxFF description for simulating reactive hydrogen and oxygen migration in BYZ-phases, we performed periodic QM simulations on a range of systems, including bulk metals, metal alloys, metal oxides, and mixed metal oxide materials. The ReaxFF development for Y, Zr, their alloys, and their oxides was discussed in ref 39. Here, we discuss only the data added to the training set to extend the potential described earlier for Y/Zr/O systems[39] to Ba/Zr/Y/O/H systems. To make this extension, QM-data were generated for the following systems:

(1) Ba phases: equations of state for the fcc, bcc, a15, and primitive cubic phases (Figure 1);

(2) BaO phases: equations of state for the fcc, primitive cubic (CsCl-type, $Pm\bar{3}m$), hexagonal ($P6_3/mmc$) and tetragonal ($P4/nmm$) (Figure 2);

(3) BaZrO$_3$ phase: equation of state for the cubic (Figure 3);

(4) BaZr$_{1-x}$Y$_x$H$_x$O$_3$ phases: relative energies for different configurations for 50% ($x = 0.5$) and 12.5% ($x = 0.125$) Y(H)-exchanged BaZrO$_3$ phases (Figure 4); and

(5) Migration barriers, as a function of O−O distance, for inter- and intraoctahedral hydrogen shift reactions (Figure 5).

The Y/Zr/O ReaxFF parameters were kept fixed to the values derived in ref 39, thus ensuring complete transferability of the force field. For all cases described in Figures 1−5, we found good agreement between the QM and ReaxFF data, indicating that ReaxFF should provide a good description of reactive hydrogen and oxygen transport in Y(H)-exchanged BaZrO$_3$

ReaxFF Reactive Force Field

J. Phys. Chem. A, Vol. 112, No. 45, 2008 **11417**

phases. Of specific importance here is that ReaxFF reproduces the QM data for the hydrogen migration barriers (Figure 5). The results in Figure 5 show that the H-migration barrier is highly dependent on the distance between the oxygen donor and acceptor atoms, indicating that the motion of these oxygen atoms is controlling hydrogen diffusion rates.

The complete set of parameters used in these simulations and a document describing the full set of potential functions are included in the Supporting Information.

4. Applications of the ReaxFF to Modeling of Hydrogen Diffusion in Y-Doped BaZrO₃

4.1. Intragrain (Single Crystal) Results. Using the ReaxFF developed here, we carried out MD simulations of the grain interior hydrogen diffusion in 12.5% BYZ (BaY$_{0.125}$H$_{0.125}$-Zr$_{0.875}$O$_3$ with 328 atoms, including 8 hydrogen atoms) at various temperatures (500, 750, 1000, 1250, and 1500 K). In these simulations, we observed that all hydrogen atoms were highly mobile. Figure 6 shows an example trajectory obtained for one of the hydrogen atoms from the simulation at $T = 1000$ K. Other such trajectories are given in the Supporting Information. These ReaxFF MD trajectories were used to calculate diffusion coefficients based on mean-square displacements (MSD) as follows:

$$\text{MSD}(m) = \langle |r(t) - r|^2 \rangle = 1/n \sum_{i=1}^{n} |r(m+i) - r(i)|^2 \quad (1)$$

where r is the position of the particle, t is the time, k is the total number of snapshots ($k = m + n > 0$), m is the maximum number of points allowed for the MSD calculation ($m = k/2$ in our calculations), n is the number of data points used for averaging, and i is the step counter.

The self-diffusion constant is obtained using the Einstein relation:

$$D = \frac{1}{6Nt} \langle |r(t) - r|^2 \rangle \quad (2)$$

where N is the number of atoms. Combining the results for various temperatures, we fit the diffusion coefficient to the form:

$$D(T) = D_0 \exp(-E_a/kT) \quad (3)$$

where E_a is the activation energy. Thus, we obtain $E_a = 0.45$ eV and $D_0 = 2.77 \times 10^{-4}$ cm^2/sec from the dependence of the hydrogen diffusion coefficient from the MD simulations as a function of temperatures (Figure 7), while the experimental values are $E_a = 0.43$ eV and $D_0 = 2.47 \times 10^{-3}$ cm^2/sec.[40]

Many of the temperatures considered in the calculations lie above the regions studied experimentally. This was an expedient
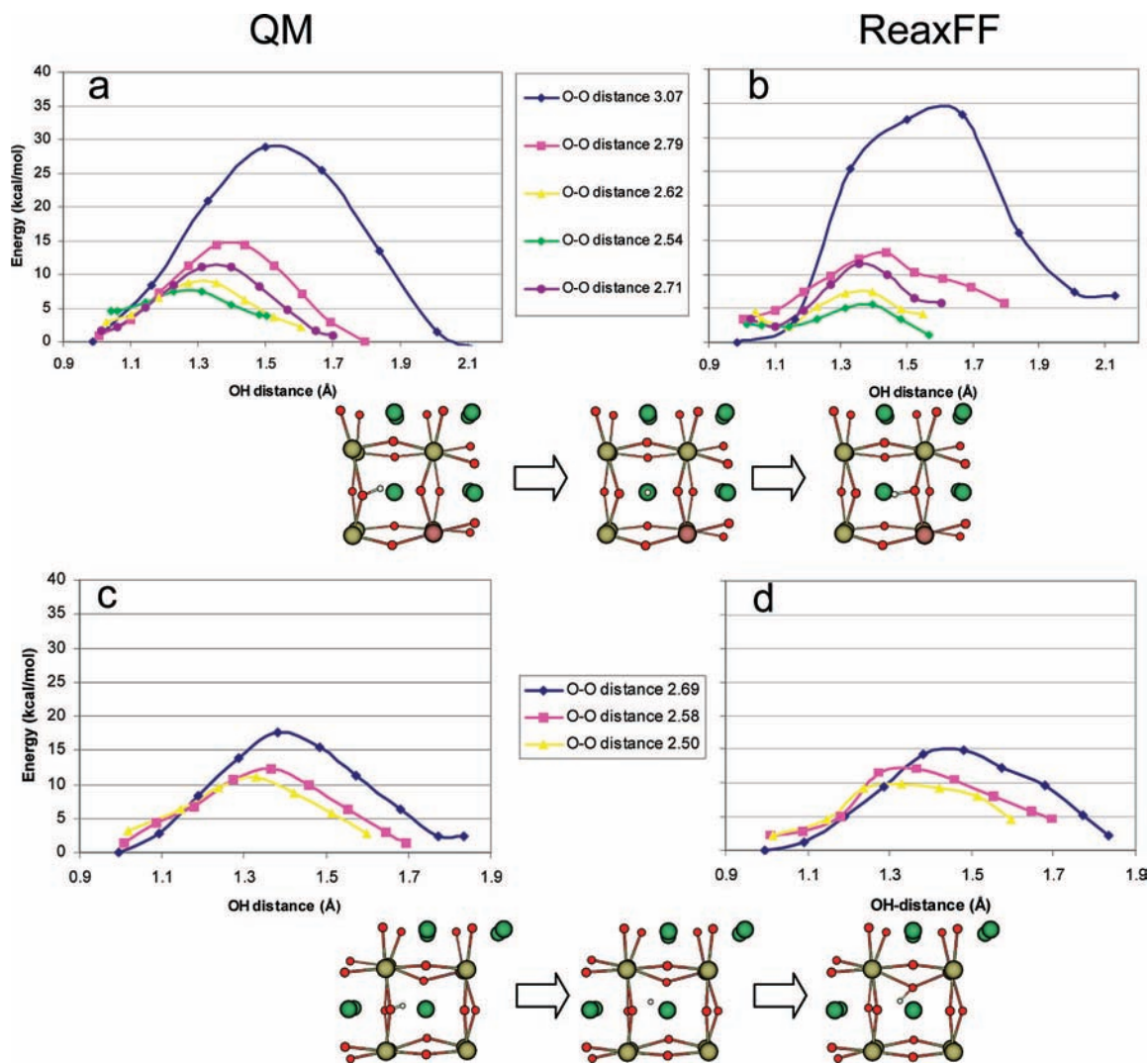
Figure 5. QM and ReaxFF barriers for inter (a,b)- and intraoctahedral (c,d) hydrogen shifts as a function of O–O distance in the 12.5%-YH-exchanged BaZrO₃ phase (Ba₈Zr₇YHO₂₄) shown as (b) in Figure 4. The interoctahedral hydrogen transfer was calculated between two O atoms, for which one is shared by two ZrO₆ octahedra while the other is shared by ZrO₆ and YO₆ octahedra. The intraoctahedral hydrogen transfer was calculated on an O–O edge of the ZrO₆-octahedron.

11418 *J. Phys. Chem. A, Vol. 112, No. 45, 2008*

van Duin et al.
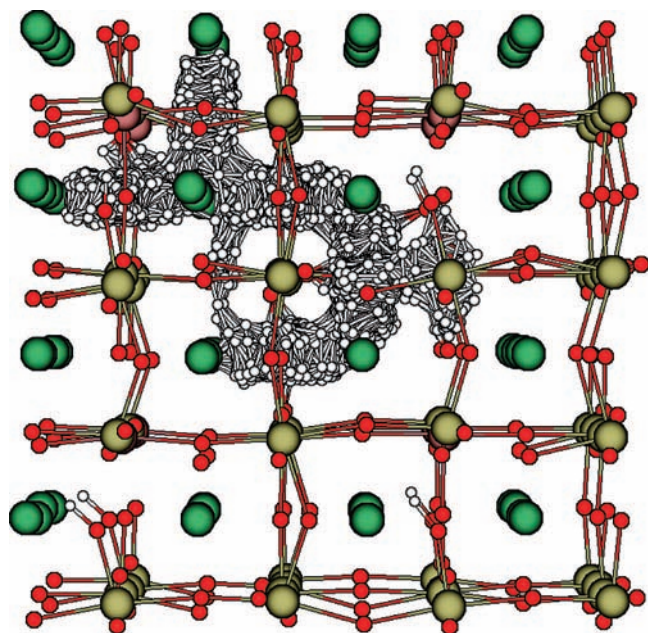
Figure 6. Trajectory of one hydrogen atom (shown by small white spheres) from ReaxFF MD simulation on Y-doped $BaZrO_3$ at $T = 1000$ K, $t = 1.5$ ns.

to reduce the computational effort for the current proof-of-concept studies. These methods can be used for much longer calculations and for many ways of defining the grain boundaries to obtain accurate predictions for various systems. Figure 7 shows the extrapolation of our higher temperature calculations to the lower temperatures of the experiments. Thus, (1) simulations at $T = 400$ K lead to $E_a = 0.45$ eV and $D = 0.6 \times 10^{-9} cm^2/sec$, while (2) experimental values at this temperature are $E_a = 0.43$ eV and $D = 8.4 \times 10^{-9} cm^2/sec$.[40]

We see that the activation energies are in excellent agreement, but the predicted diffusion coefficient D at this temperature (400 K) is $14 \times$ lower than experiment. This may be because our simulations were performed for the ideal stoichiometric structures ($BaY_{0.125}H_{0.125}Zr_{0.875}O_3$), whereas the experimental data are for the nonstoichiometric $BaZr_{0.9}Y_{0.1}O_{3-\delta}$ compound that contains oxygen vacancies. This would lead to a lower D than experiment. It may be necessary to carry out ReaxFF MD simulations at lower temperatures to determine whether there may be other explanations of the discrepancy.

Münch et al. have reported proton diffusion in some perovskites, including $BaZrO_3$,[41] using the quantum MD simulations. However, the total number of atoms was 138, including three protonic defects. They found $E_a = 0.83 \pm 0.65$ eV and $D_0 \approx 5 \times 10^{-4}$ cm²/sec, which are significantly different from experiment.

4.2. Effect of Grain Boundaries on H Diffusion. As mentioned above, the experimental proton conductivity of various sized nanocrystals suggests that the grain boundaries in BYZ reduce the conductivity by $\sim100\times$ compared to bulk single crystal values. To investigate this phenomenon, we performed ReaxFF MD simulations on a BYZ structure, in which the grain boundaries were generated by twisting (111) and (110) grains by 35.26° along the $<1\bar{1}0>$ direction (Figure 8). These choices were motivated by experimental high-resolution transmission electron microscopy results.[42] Our model structure is a periodic 872-atom box ($40.00 \times 21.22 \times 18.02$ Å) that includes 16 hydrogen and Y atoms. The two grains were initially separated each from other by about 5 Å and then allowed to relax. Periodic boundary conditions were applied along all directions. As seen in Figure 8, this leads to a low
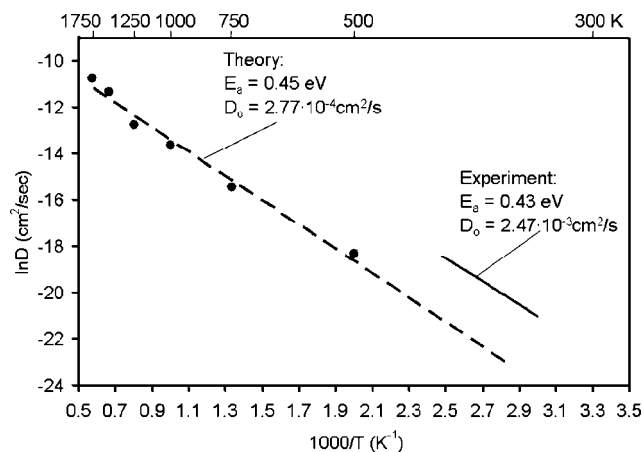

Figure 7. Calculated hydrogen diffusion coefficient for crystalline Y-doped $BaZrO_3$. This would correspond to the intragranular diffusion in a polycrystalline system. The experimental data are for $BaZr_{0.9}Y_{0.1}O_{3-\sigma}$ and were extracted from Figure 10 in ref 40. The very similar activation energy suggests that ReaxFF is correctly describing the rate determining step. The $9\times$ higher value for D_0 in the experiment suggests that the experimental system might have more disorder and additional defects.
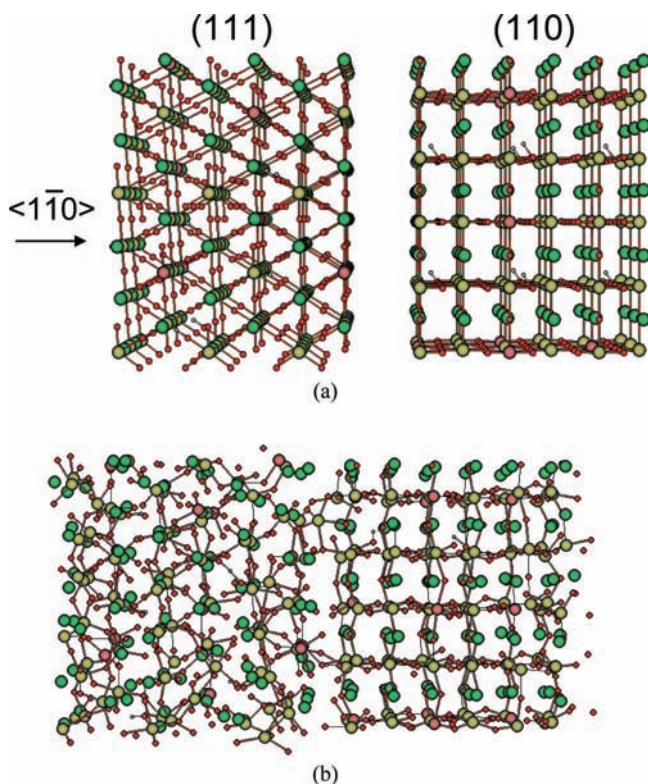
Figure 8. Model of the grain boundary in Y-doped $BaZrO_3$. Both grains have the same $<1\bar{1}0>$ axis (horizontal) but the left grain has the (111) plane at the top while the right one has (110) at the top. The system is periodic in 3D, using just the unit cell shown above. (a) Starting point for constructing the computer model with grain boundaries. The initial separatation between the grains was 5.0 Å. (b) The equilibrated structure obtained from 200 ps of MD simulation at 300 K.

density in the grain boundary region, which is consistent with an experimental result.[7] The refractory nature of BYZ makes it difficult to process to a high density.

Using this input structure, we performed MD simulations at various temperatures (800, 900, 1000, 1250, 1500, 1750, and 2000 K). These simulations found a severely reduced hydrogen

ReaxFF Reactive Force Field

J. Phys. Chem. A, Vol. 112, No. 45, 2008 **11419**
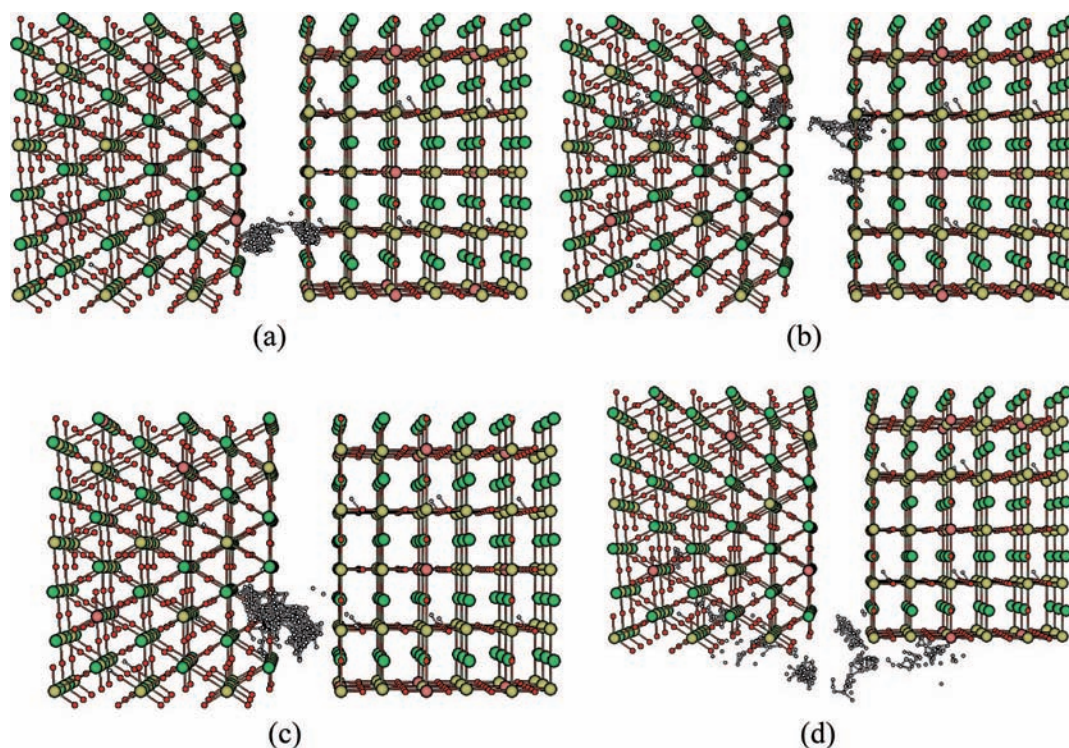
Figure 9. Trajectories over 200 ps for all 16 hydrogen atoms in Y-doped BaZrO$_3$ with grain boundaries, obtained from the ReaxFF MD simulations at T = (a) 1250, (b) 1500, (c) 1750, and (d) 2000 K.

mobility in the grain boundary. Thus, at temperatures 1250 K and below, we found that 200 ps of MD simulations led to no hydrogen atoms diffusing across the grain boundary. Thus, Figure 9a shows the migration of all 16 H atoms at 1250 K. In contrast, Figure 9b at 1500 K shows that one hydrogen in the left grain moves into the right one. Similarly, the trajectories in Figure 9, parts c and d, for 1750 and 2000 K show two and four H atoms moving from one grain to the other.

To quantify these hopping rates, we estimated the residence time of the hydrogen inside the grain boundary by detailed observation of full trajectories for hydrogen atoms to diffuse across grain boundaries. This leads to residence times of $\tau_{res} \approx$ 80 ps at 1500 K, ~40 ps at 1750 K, and ~20 ps at 2000 K. Figure 10 plots these results, leading to an effective activation energy of 0.71 eV. These results indicate that the grain boundaries decrease dramatically the total proton conductivity of BYZ, in agreement with experimental data.[4,41] We expect that simulations for longer time would observe proton transport across the grain-boundary at lower temperatures.

On the basis of the MD-trajectories for various temperatures, we calculated diffusion coefficients and activation energy for the hydrogen transport in the BYZ system with grain boundaries. Figure 11a compares our results with experimental data.[42] Here, we see that simulation results are in the experimental range for hydrogen diffusion. Thus, we calculate E_a = 0.66 eV and D_0 = 3.506×10^{-3} cm^2/s for hydrogen diffusion with 1.5 nm grain size, which is comparable to E_a = 0.54 eV and D_0 = 0.70×10^{-5} cm^2/s from IS (impedance spectroscopy) experiments for BYZ with a grain size of 10 nm.

The differences between theory and experiments might be because our BYZ model has much smaller grains than experiment, leading to much larger grain boundary areas. We note here the calculated activation energy (0.66 eV) from Figure 11a is close to the value (0.71 eV) obtained from the temperature dependence of the residence time of hydrogen in the grain boundaries (Figure 10).
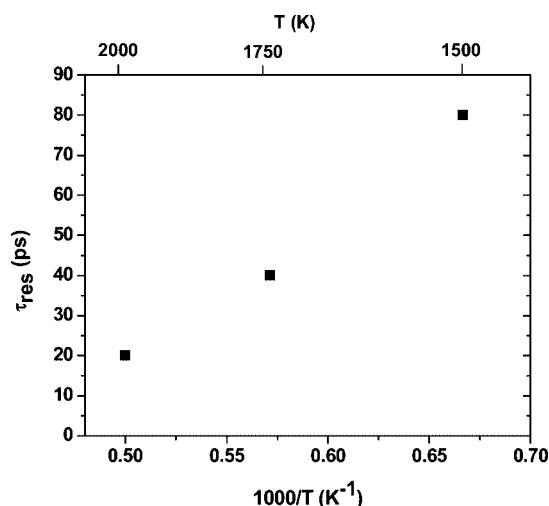
Figure 10. Temperature-dependent residence time of the hydrogen atoms in the Y-doped BaZrO$_3$ grain boundaries. From this result, a line of ln τ_{res} vs 1000/T has the relationship ln τ_{res} = −28.72 851 + 8.26 138 × 10^3/T.

The predicted E_a = 0.66 eV for hydrogen diffusion in the BYZ system with grain boundaries is higher than the E_a = 0.45 eV for the grain interior hydrogen diffusion (Figure 11b). We estimated the activation energy for the hydrogen diffusion only inside grain-boundary cores of BYZ by considering the MSD of hydrogen atoms to stay only in the grain boundary core. These results are shown in Figure 11b, leading to E_a = 1.12 eV and D_0 = 5.260×10^{-3} cm^2/s. This value is higher than that of 0.70 eV obtained by Bohn and Schober from electrochemical impedance measurements of hydrogen diffusion in grain boundaries of BaZr$_{0.9}$Y$_{0.1}$O$_{3-\delta}$.[4] This discrepancy might be because our simulations consider only one type of the grain boundary structure (twisted), whereas many other types (for example, tilt grain boundaries) can occur in perovskite oxides.[43] In addition,

(a)

(b)
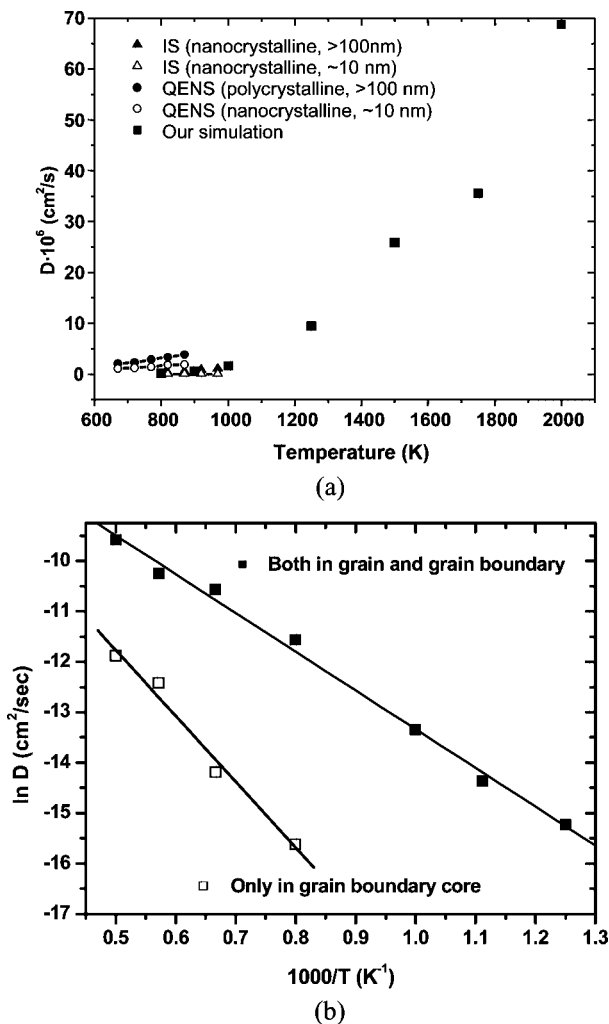
Figure 11. (a) Hydrogen diffusion coefficients of single crystal Y-doped BaZrO$_3$. ReaxFF calculations (solid squares) lead to $D_0 = 3.506 \times 10^{-3}$ cm^2/s and $E_a = 0.66$ eV. The experimental values are for two sizes of grains (10 and 100 nm) and from two types of experiments, IS (impedance spectroscopy)[4] and QENS (quasi-elastic neutron scattering).[42] (b) Calculated hydrogen diffusion coefficients both in grains and grain boundaries (solid squares) and only inside grain boundaries (open squares). This leads to $D_0 = 5.260 \times 10^{-3}$ cm^2/s and $E_a = 1.12$ eV.

we grew this grain boundary just once; a more thorough study would grow it many times, perhaps using Monte Carlo techniques to reequilibrate the grain boundary studies.

Indeed, our preliminary calculations for the tilt grain boundaries in BYZ show a lower resistivity with increased hydrogen diffusion as compared with the twist grain boundary.

4.3. Oxygen Diffusion. Figure 12 compares our computed oxygen diffusion in BYZ with IS experiments on BaZr$_{0.9}$Y$_{0.1}$O$_{3-\delta}$ crystals, where we see good agreement:

(1) simulations: $E_a = 0.95$ eV and $D_0 = 7.152 \times 10^{-3}$ cm^2/s, and
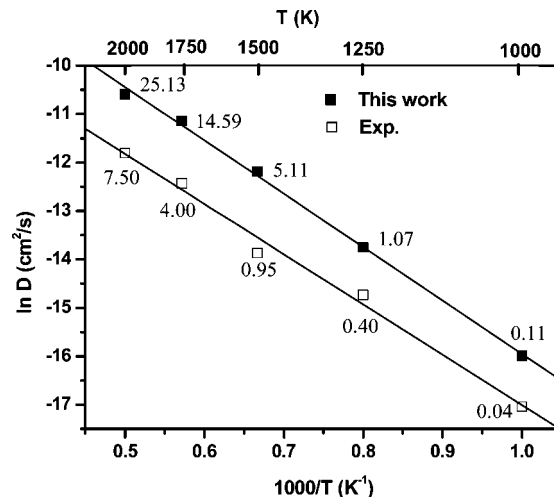
(2) experiment: $E_a = 0.89$ eV and $D_0 = 1.309 \times 10^{-3}$ cm^2/s;[44]

Our calculated diffusion coefficients are as follows:

(1) $D(O) = 0.11 \times 10^{-6}$, as compared to $D(H) = 1.59 \times 10^{-6}$ cm^2/s at 1000 K; and

(2) $D(O) = 1.07 \times 10^{-6}$ cm^2/s, as compared to $D(H) = 6.71 \times 10^{-6}$ cm^2/s at 1250 K.

Thus, the calculated ratio is $D(H)/D(O) = 16$ at 1000 K, 6 at 1250 K, 5 at 1500 K, and 3 at 1750 and 2000 K. This oxygen

Figure 12. Oxygen diffusion coefficients for Y-doped BaZrO$_3$. The ReaxFF simulations lead to $E = 0.95$ eV and $D_0 = 7.152 \times 10^{-3}$ cm^2/s, while impedance spectroscopy experiments lead to $E_a = 0.89$ eV and $D_0 = 1.309 \times 10^{-3}$ cm^2/s for BaZr$_{0.9}$Y$_{0.1}$O$_{3-\delta}$ samples.[37] The values inside of the figure indicate the actual diffusion coefficients ($\times 10^{-6}$ cm^2/s).

diffusion becomes significant and comparable to the hydrogen diffusion above 1250 K. Further investigations of the diffusion parameters as well as analyzing the grain boundary structures in detail are planned.

4.4. Interpretation. *4.4.1. Oxygen Distributions.* As a first step toward interpreting these results, Figure 13a shows the O−O radial distribution function (RDF) and integrated number of neighbors (Figure 13b) for the 12.5% BYZ alloy without grain boundaries. This is compared with the results for the system with grain boundaries (Figure 13c, d). Here, we find average O−O separations (averaged over the first peak) as follows:

(1) 3.07 Å for 12.5% BYZ alloy without grain boundaries (4 near O neighbors).

(2) 3.37 Å (9.5 near O neighbors) for the 180 O at the grain boundary, and a peak at 2.85 Å (2.0 near O neighbors), probably due to distortion of the oxygen network at the grain boundary.

(3) 3.09 Å (3.7 near O neighbors) for the 316 O not at the grain boundary.

Thus, the O−O distance over which H at the grain boundary must hop is 0.3 Å longer than the distance they must hop in the bulk grain. Since the hopping rate (Figure 5) decreased rapidly as the O−O separation is increased, the reduced diffusion of protons across the grain boundary may arise from the increased average distances between oxygen atoms in the interface.

This result suggests a strategy for improving the grain boundary hopping of hydrogens and, hence, the overall H diffusion of multigranular BYZ. If the critical issue in the grain boundary diffusion is the increased O−O separations, then the performance of BYZ for multigranular systems might be improved with small amounts of additives chosen to pull the oxygen atoms together when precipitated to the grain boundaries. Here, we might consider small amounts of larger trivalent ions, such as La or Lu, or of tetravalent ions, such as Hf or Th. The idea is that these ions might prefer the grain boundaries, just as it is observed for Zn in ZnO-modified barium zirconate,[7] but lead to tighter O−O distances that would decrease the barriers for hydrogen migration.

4.4.2. Metal Distributions. The distribution of Ba, Zr, Y, and O have been analyzed in various slabs (slab thickness = 0.05

ReaxFF Reactive Force Field

J. Phys. Chem. A, Vol. 112, No. 45, 2008 **11421**
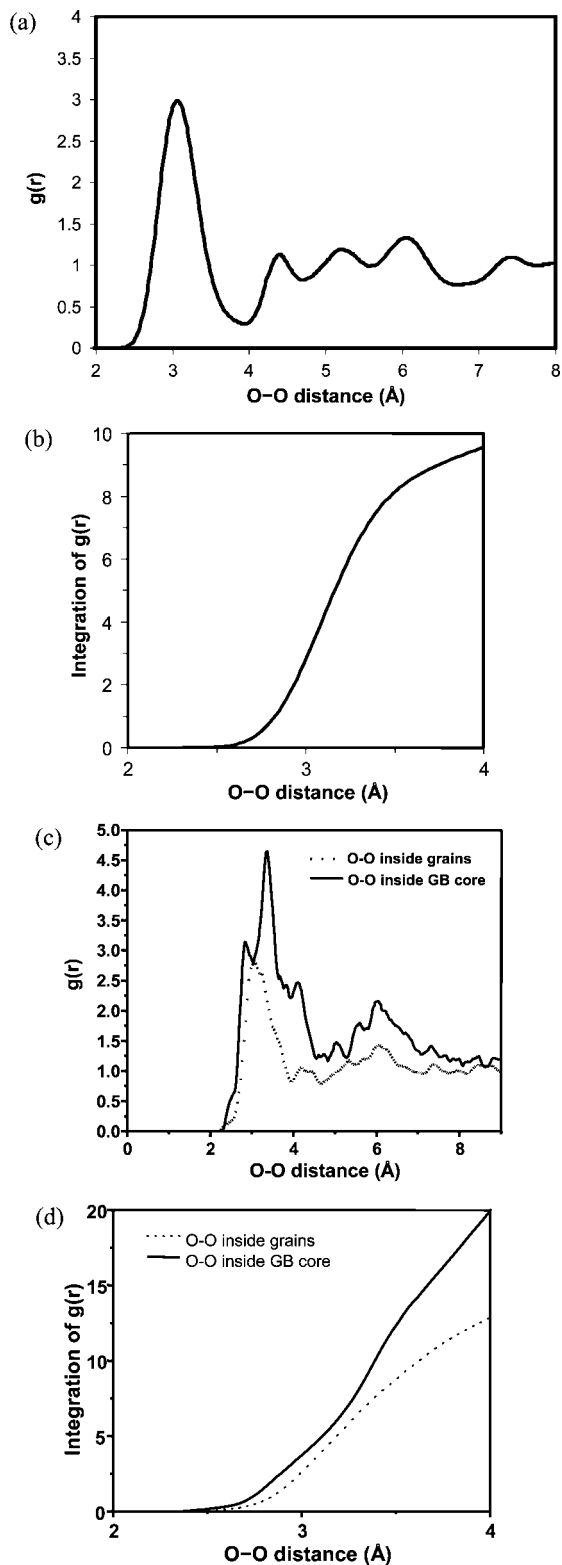
Figure 13. Radial O−O distribution function $g(r)$ and its integration for 12.5% Y-doped $BaZrO_3$ without grain boundaries (a, b) and with grain boundaries (c, d).

Å) cut along the x-axis, which is parallel to the $<1\bar{1}0>$ direction in Figure 8a. As the temperature increases, we find that Ba, Zr, Y, and O all diffuse into grain boundary cores where especially oxygen atoms are uniformly distributed. In the central part of the grain boundary, we identify atomic compositions of the following:

(1) $Ba_{54}Zr_{37}Y_3H_1O_{91}$ ($\approx Ba_{1.35}Zr_{0.92}Y_{0.08}H_{0.03}O_{2.28}$) at 550 K,

(2) $Ba_{59}Zr_{39}Y_5H_2O_{111}$ ($\approx Ba_{1.34}Zr_{0.89}Y_{0.11}H_{0.05}O_{2.52}$) at 1000 K,

(3) $Ba_{50}Zr_{42}Y_5H_5O_{115}$ ($\approx Ba_{1.06}Zr_{0.89}Y_{0.11}H_{0.11}O_{2.45}$) at 1500 K, and

(4) $Ba_{49}Zr_{46}Y_5H_5O_{116}$ ($\approx Ba_{0.96}Zr_{0.90}Y_{0.10}H_{0.10}O_{2.27}$) at 2000 K.

Thus, at low temperature, Ba atoms are in excess, and O atoms are deficient in the grain boundaries relative to grain interiors, whereas for higher temperatures, the Ba is no longer in excess, but the oxygen remains deficient.

4.4.3. Charge Distributions. We also analyzed the average charge distribution in various slabs (slab thickness = 0.05 Å) of an equilibrated BYZ crystal at different temperatures along the x direction. We find an average charge over the grain boundary as follows:

(1) $+4.66 \times 10^{-2}$ $e/Å^2$ at 550K,

(2) $+4.80 \times 10^{-2}$ $e/Å^2$ at 1000 K,

(3) $+2.60 \times 10^{-2}$ $e/Å^2$ at 1500K, and

(4) $+3.54 \times 10^{-2}$ $e/Å^2$ at 2000 K.

This positive net charge arises from the deficiency of oxygen atoms in the grain boundary. The result is an increased average O−O distance and a repulsive interaction between the grain boundary and hydrogen atoms, both of which would lead to slower hydrogen diffusion through the grain boundary and the observed high grain boundary resistance for this hydrogen diffusion.[4,45]

5. Conclusions

These studies validate that MD with ReaxFF provides a description of the diffusion of protons in the bulk BYZ phase and across grain boundaries, in reasonable agreement with experimental diffusion measurements. With this validation, we can now use the ReaxFF MD trajectories to understand the atomic origin of the phenomena.

These calculations suggest that the reduced diffusion of protons across the grain boundary may result from increased average distances between oxygen atoms in the interface, which necessarily leads to larger barriers for proton hopping. This suggests a strategy for improving the diffusion performance of multigranular BYZ: find additives that would tend to precipitate to the grain boundary while pulling oxygen atoms closer. Possibilities might be to use a small amount of larger trivalent ions such as La or Lu or of tetravalent ions such as Ce, Hf, or Th.

ReaxFF has also been shown to accurately describe the reactive processes on the electrodes.[17,46] This sets the stage for using ReaxFF MD to simulate the overall performance of these fuel cell systems,[15] including

(1) the interfacial processes as the fuel reacts at the anode to provide protons to the membrane,

(2) the diffusion of the protons across the multigranular electrolyte, and

(3) the interfacial processes as the protons reduce the O_2 at the cathode to form H_2O.

At the same time, these simulations could be used to predict the effects of CO poisoning of the anode, the crossover of fuel to the cathode and the crossover of H_2O and O_2 to the anode, and perhaps the production of reactive intermediates that might lead to degradation of the catalyst or membrane. Thus, ReaxFF MD should enable the simulations needed to provide an atomistic understanding of performance of these systems. This should eventually allow the simulations to test new strategies for improving performance. The parameter device from such

studies could then be used to provide the macroscopic parameters for continuum simulations of overall fuel cell performance.

Supporting Information Available: ReaxFF parameters developed in this paper, ReaxFF potential functions, trajectories for mobile hydrogen atoms, and atomic coordinates of the structures shown in Figure 4. This information is available free of charge via the Internet at http://pubs.acs.org.

References and Notes

(1) Iwahara, H.; Uchida, H.; Tanaka, S. *Solid State Ionics* **1983**, *9−10*, 1021.

(2) Iwahara, H.; Uchida, H.; Ono, K.; Ogaki, K. *J. Electrochem. Soc.* **1988**, *135*, 529.

(3) Kreuer, K.-D.; Adams, S.; Munch, W.; Fuchs, A.; Klock, A.; Maier, J. *Solid State Ionics* **2001**, *145*, 295.

(4) Bohn, H. G.; Schober, T. *J. Am. Ceram. Soc.* **2000**, *83*, 768.

(5) Haile, S. M.; Staneff, G.; Ryu, K. H. *J. Mat. Sci.* **2001**, *36*, 1149.

(6) Coors, W. G.; Readey, D. W. *J. Am. Ceram. Soc.* **2002**, *85*, 2637.

(7) Babilo, P.; Haile, S. M. *J. Am. Ceram. Soc.* **2005**, *88*, 2362.

(8) Iguchi, F.; Sata, N.; Tsurui, T.; Yugami, H. *Solid State Ionics* **2007**, *178*, 691.

(9) van Duin, A. C. T.; Dasgupta, S.; Lorant, F.; Goddard, W. A. *J. Phys. Chem. A* **2001**, *105*, 9396.

(10) Strachan, A.; van Duin, A. C. T.; Chakraborty, D.; Dasgupta, S.; Goddard III, W. A. *Phys. Rev. Lett.* **2003**, *91*, 098301.

(11) Strachan, A.; Kober, E. M.; van Duin, A. C. T.; Oxgaard, J.; Goddard III, W. A. *J. Chem. Phys.* **2005**, *122*, 054502.

(12) van Duin, A. C. T.; Zeiri, Y.; Dubnikova, F.; Kosloff, R.; Goddard III, W. A. *J. Am. Chem. Soc.* **2005**, *127*, 11053.

(13) Chenoweth, K.; Cheung, S.; van Duin, A. C. T.; Goddard III, W. A.; Kober, E. M. *J. Am. Chem. Soc.* **2005**, *127*, 7192.

(14) Goddard, W. A.; van Duin, A. C. T.; Chenoweth, K.; Cheng, M. J.; Pudar, S.; Oxgaard, J.; Merinov, B.; Jang, Y. H.; Persson, P. *Top. Catal.* **2006**, *38*, 93.

(15) Goddard, W.; Merinov, B.; van Duin, A.; Jacob, T.; Blanco, M.; Molinero, V.; Jang, S. S.; Jang, Y. H. *Mol. Simul.* **2006**, *32*, 251.

(16) Buehler, M. J.; van Duin, A. C. T.; Goddard, W. A. *Phys. Rev. Lett.* **2006**, *96*, 095505.

(17) Ludwig, J.; Vlachos, D. G.; van Duin, A. C. T.; Goddard, W. A. *J. Phys. Chem. B* **2006**, *110*, 4274.

(18) Cheung, S.; Deng, W. Q.; van Duin, A. C. T.; Goddard, W. A. *J. Phys. Chem. A* **2005**, *109*, 851.

(19) Nielson, K. D.; van Duin, A. C. T.; Oxgaard, J.; Deng, W. Q.; Goddard, W. A. *J. Phys. Chem. A* **2005**, *109*, 493.

(20) Zhang, Q.; Cagin, T.; van Duin, A. C. T.; Goddard, W. A.; Qi, Y.; Hector, L. G. *Phys. Rev. B* **2004**, *69*, 045423.

(21) Chenoweth, K.; van Duin, A.C.T.; Goddard, W.A. *J. Am. Chem. Soc.*, submitted.

(22) Nakano, A.; Kalia, R. K.; Nomura, K.; Sharma, A.; Vashishta, P.; Shimojo, F.; van Duin, A. C. T.; Goddard, W. A.; Biswas, R.; Srivastava, D. *Comput. Mater. Sci.* **2007**, *38*, 642.

(23) Perdew, J. P.; Burke, K.; Ernzerhof, M. *Phys. Rev. Lett.* **1996**, *77*, 3865.

(24) Ceperley, D. M.; Alder, B. J. *Phys. Rev. Lett.* **1980**, *45*, 566.

(25) Perdew, J. P.; Zunger, A. *Phys. Rev. B* **1981**, *23*, 5048.

(26) Slater, J. C. Quantum Theory for Molecules and Solids. *The Self-Consistent Field for Molecules and Solids*; McGraw-Hill: New York, 1974; Vol. *4*.

(27) Becke, A. D. *Phys. Rev. A* **1988**, *38*, 3098.

(28) Vosko, S. H.; Wilk, L.; Nusair, M. *Can. J. Phys.* **1980**, *58*, 1200.

(29) Lee, A.; Yang, W.; Parr, R. G. *Phys. Rev. B* **1988**, *37*, 785.

(30) Koch W.; Holthausen, M. C. *A Chemist's Guide to Density Functional Theory*; Wiley-VCH: Weinheim, 2001.

(31) Mattsson, A. E.; Schultz, P. A.; Desjarlais, M. P.; Mattsson, T. R.; Leung, K. *Model. Simul. Mater. Sci. Eng.* **2005**, *13*, R1.

(32) Jaguar 5.0, Schrodinger Inc., Portland, OR, 2000.

(33) Hay, P. J.; Wadt, W. R. *J. Phys. Chem.* **1985**, *82*, 299.

(34) Goddard III, W. A. *Phys. Rev.* **1968**, *174*, 659.

(35) Melius, C. F.; Goddard III, W. A. *Phys. Rev. A* **1974**, *10*, 1528.

(36) Francl, M. M.; Pietro, W. J.; Hehre, W. J.; Binkley, J. S.; Gordon, M. S.; DeFrees, D. J.; Pople, D. J. *J. Chem. Phys.* **1982**, *77*, 3654.

(37) SchultzP. A. Unpublished results (a description of the method is in Feibelman, P. *J. Phys. Rev. B* **1987**, *35*, 2626.

(38) Schultz, P.A. unpublished; see http://dft.sandia.gov/Quest.

(39) Duin, A.C.T.; Merinov, B.V.; Jang, S.S.; Goddard, W.A. *J. Phys. Chem.*, submitted for publication.

(40) Kreuer, K.-D. *Annu. Rev. Mater. Res.* **2003**, *33*, 333.

(41) Münch, W.; Kreuer, K.-D.; Seifert, G.; Maier, J. *Solid State Ionics* **2000**, *136−137*, 183.

(42) Groβ, B.; Beck, C.; Meyer, F.; Krajewski, T.; Hempelmann, R.; Altgeld, H. *Solid State Ionics* **2001**, *145*, 325.

(43) Browning, N. D.; Moltaji, H. O.; Buban, J. P. *Phys. Rev. B* **1998**, *58*, 8289.

(44) Kreuer, K.-D. *Solid State Ionics* **1999**, *125*, 285.

(45) Nomura, K.; Kageyama, H. *Solid State Ionics* **2007**, *178*, 661.

(46) Sanz-Navarro, C.; Astrand, P.; Chen, D.; Ronning, M.; van Duin, A. C. T.; Jacob, T.; Goddard, W. A. *J. Phys. Chem. A* **2008**, *112*, 1392.

(47) Liu, L.-G. *J. Appl. Phys.* **1971**, *42*, 3702.